MATERIALS CHEMISTRY FRONTIERS

RESEARCH ARTICLE

View Article Online
View Journal | View Issue

Cite this: *Mater. Chem. Front.*, 2021, **5**, 6052

Graphdiyne anchored ultrafine Ag nanoparticles for highly efficient and solvent-free catalysis of CO_2 cycloaddition†

Chang Liu, Chao Zhang and Tong-Bu Lu *

Received 5th May 2021,
Accepted 19th June 2021

DOI: 10.1039/d1qm00672j

rsc.li/frontiers-materials

Apart from photo-/electro-catalytic CO_2 reduction, an important alternative route to CO_2 utilization is to use this inert molecule as a C1 source to synthesize value-added chemicals; however, the practical application is limited by the low conversion efficiency. Herein, we reported a composite catalyst of 3D sponge-like pyrenyl-graphdiyne (Pyr-GDY) anchored ultrafine Ag nanoparticles (Ag/Pyr-GDY), with the average size of Ag NPs of only 1.6 nm. The porous 3D Pyr-GDY component can not only anchor and stabilize the capping agent free ultrafine Ag NPs by virtue of the strong affinity between alkynyl groups and Ag, but also enhance the local concentration of CO_2 due to the porous nature of 3D Pyr-GDY. As a result, the optimized Ag/Pyr-GDY catalyst displays a record-high activity towards the catalysis of CO_2 cycloaddition with propargylamines under ambient temperature and pressure, with a TON of 20 488 and a yield of 83%, and is 15.3 times more active than the most efficient catalyst Ag27-MOF (TON = 1333, yield = 34%). Moreover, our catalysis was performed in a solvent-free system, which provides an economic, green and practical avenue for carbon capture, utilization and storage (CCUS).

1. Introduction

The overdependence on fossil fuels has led to excessive emission of CO_2 into the atmosphere,[1,2] and scientists have been exploring different routes to neutralize the CO_2 emission and in the meantime to obtain value-added products. Aside from photo-/electro-/bio-chemical pathways,[3–30] CO_2 can be employed as a C1 source to participate in the cycloaddition reaction with propargylamines,[31–33] haloalkylamines,[34] and aziridines[31,33] for the production of 2-oxazolidinones. Many metal-based catalysts such as Cu,[35–39] Co,[40] Zn,[41] Pd,[42–46] Ag,[36,37,47–57] Pt,[36] and Au[37,58–63] have been found to be catalytically active for this reaction, among which Ag-based catalysts have attracted broad interest for their capability of promoting the reaction under mild conditions due to their soft π-Lewis acid characteristic. For example, Duan *et al.* assembled Ag clusters with thiourea-incorporating ligands and obtained two metal–organic frameworks (MOFs) of TOS-Ag4 and TNS-Ag8. They found that a catalyst loading of merely 0.1 mol% could effectively promote the conversion of propargylamines to oxazolidinones in the presence of 1 bar CO_2 at room temperature, with turnover numbers (TONs) of 930 and 760, respectively.[55] Recently, Sun *et al.* reported a very efficient Ag-cluster-based MOF catalyst denoted as Ag27-MOF, which can efficiently catalyze the cycloaddition of both terminal and internal propargylamines with CO_2 under atmospheric pressure in acetonitrile, with a maximum TON of 1333.[49] These successes shed light on the design of Ag-based high-performance heterogeneous catalysts for CO_2 cycloaddition reaction. However, the catalytic activities of the reported Ag-based catalysts are still too low for practical applications. Moreover, most of the CO_2 cycloaddition reactions were performed in organic solvents, which consumed enormous amounts of solvents and energy in the subsequent separation process to get pure products. It is still highly desired to develop more efficient CO_2 cycloaddition catalysts, especially to catalyze the reactions in a solvent-free system.

The low catalytic performance of Ag cluster/NP-based catalysts may partly originate from the presence of surface capping agents, as most of the Ag clusters/NPs should be stabilized by the capping agents to prevent aggregation, while the coordination between the Ag clusters/NPs and the capping ligands will block part of the catalytic sites of Ag clusters/NPs, thus decreasing their catalytic activity. One can expect that the catalytic activity of Ag NP-based catalysts could be enhanced by decreasing or without using the capping agents. However, it remains a great challenge to construct such stable capping agent free ultrafine Ag NPs, as the ultrafine Ag NPs strongly tend to aggregate without the stabilization of surface capping agents.

Recently, graphdiyne (GDY), which was first synthesized by the Li group in 2010,[64] has attracted considerable attention.

A MOE International Joint Laboratory of Materials Microstructure, Institute for New Energy Materials and Low Carbon Technologies, School of Materials Science and Engineering, Tianjin University of Technology, Tianjin 300384, China. E-mail: lutongbu@tjut.edu.cn

† Electronic supplementary information (ESI) available. See DOI: 10.1039/d1qm00672j

GDYs are generally synthesized *via* Cu-catalyzed polymerization of aromatic monomers with multiple terminal alkynyl groups, and feature a unique π-conjugated two-dimensional (2D) structure made of sp- and sp^2-hybridized carbon atoms.[65,66] In 2019, we synthesized a pyrenyl-graphdiyne (Pyr-GDY) carbon material,[67] which featured a three-dimensional (3D) architecture composed of crossover nanowires, with abundant uncoupled terminal alkynes on the surface of nanowires,[67,68] which could act as the reduction sites for electroless deposition of sub-nanometric metal particles.[67] We envisage that the capping agent free ultrafine Ag NPs would be *in situ* formed by the reduction of terminal alkynyl groups, and stabilized by Pyr-GDY through a strong interaction between Ag NPs and the conjugated diacetylene and terminal alkynyl groups.

Herein, we reported a Pyr-GDY anchored capping agent free ultrafine Ag NP composite catalyst of Ag/Pyr-GDY, with the average size of Ag NPs as small as 1.6 nm. To our knowledge, such small Ag NPs without capping agents have not been documented so far. As expected, Ag/Pyr-GDY displays outstanding and solvent-free catalytic activity for CO_2 cycloaddition with propargylamines under ambient temperature and pressure, with record TONs of 20 488 (83% conversion) and 10 971 (100% conversion), respectively, 15.3 times higher than the most efficient catalyst of Ag27-MOF (achieved a maximum TON of 1333 with a 34% conversion in acetonitrile solvent).[49] Such a high catalytic activity can be attributed to the sponge-like porous 3D Pyr-GDY component, which can disperse and stabilize the capping agent free ultrafine Ag NPs through the strong interactions between alkynyl groups and Ag NPs, as well as the strong CO_2 affinity of 3D sponge-like porous Pyr-GDY.

2. Results and discussion

Synthesis and structural characterization

Cu/Pyr-GDY was synthesized *via* the Glaser–Hay coupling reaction. Cu(II) acetate was selected as the catalyst to catalyze the terminal alkyne coupling of the 1,3,6,8-tetraethynylphrene (TEP) monomer to get the Cu/Pyr-GDY product as a dark brown powder (Fig. 1a), in which single-atom Cu and ultrafine Cu NPs were formed *in situ* and anchored in porous Pyr-GDY. The SEM (Fig. 2a) and high-resolution transmission electron microscopy (HRTEM) images (Fig. S1a–c, ESI†) show that the morphology of Cu/Pyr-GDY is a 3D sponge-like porous structure composed

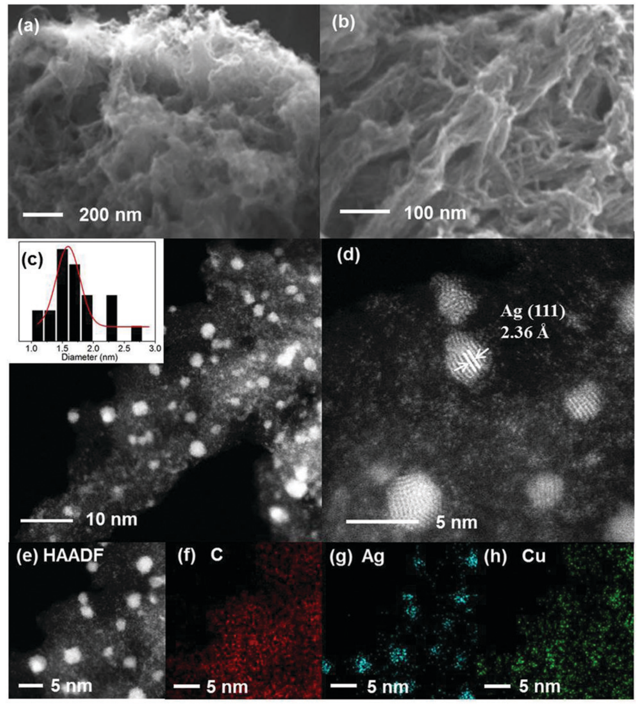

Fig. 2 (a and b) SEM images for Cu/Pyr-GDY (a) and Ag/Pyr-GDY-5.3 (b). (c and d) HAADF-STEM images of Ag/Pyr-GDY-5.3 at different magnifications; the size distribution of Ag NPs is shown (c, inset), the lattice fringes of Ag NP are shown in (d). (e–h) HAADF-STEM elemental mapping images of Ag/Pyr-GDY-5.3.

of tightly cross-connected nanowires. The aberration-corrected high-angle annular dark-field scanning transmission electron microscopy (HAADF-STEM) images of Cu/Pyr-GDY show that both ultrafine Cu NPs and Cu single atoms coexist on the surface of Cu/Pyr-GDY, with the size of ultrafine Cu NPs less than 1.0 nm (Fig. S1d–f, ESI†). The HAADF-STEM elemental mapping images (Fig. S1g–i, ESI†) of Cu/Pyr-GDY reveal that C and Cu are evenly distributed over the sample. The Raman spectrum of Cu/Pyr-GDY (Fig. S1j, ESI†) shows five peaks: the peak at 1236 cm^{-1} corresponds to the C–H in-plane bending vibration, and the peaks at 1369, 1495 and 1610 cm^{-1} correspond to the C–C stretching vibration of the pyrene ring. Notably, the characteristic peak at 2178 cm^{-1} confirms the presence of conjugated diacetylene links in Cu/Pyr-GDY. The peak around 1973 cm^{-1} belonging to the terminal uncoupled alkynyl group[67] is hardly observed, indicating that most of terminal alkynyl groups were coordinated to Cu or/and coupled to form diacetylene links in Cu/Pyr-GDY. X-Ray photo-electron spectroscopy (XPS) is conducted for Cu/Pyr-GDY, and the C 1s peak can be deconvoluted into four sub-peaks at 284.6, 285.2, 286.6 and 288.5 eV, respectively (Fig. S1k, ESI†), which correspond to the binding energies of C=C (sp^2), C≡C (sp), C–O, and C=O bonds, respectively. The band area of the sp^2-hybridized carbon is almost twice as much as that of the sp-hybridized carbon, which is consistent with the ideal structure of Cu/Pyr-GDY. The XPS pattern of Cu 2p for Cu/Pyr-GDY shows two peaks at 933.4 and 953.2 eV (Fig. S1l, ESI†), which

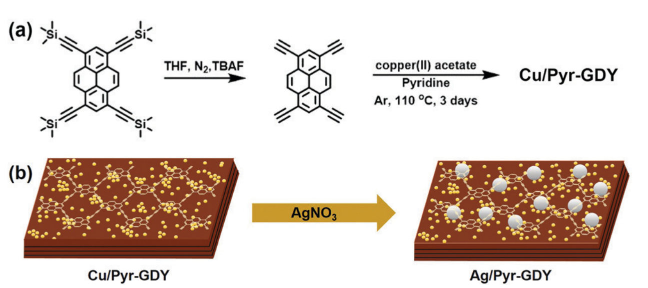

Fig. 1 Schematic illustrations for the synthesis of Cu/Pyr-GDY (a), and Ag/Pyr-GDY-*x* (b).

can be assigned to either Cu^+ or Cu^0.[69] The N_2 adsorption–desorption experiment was carried out at 77 K for Cu/Pyr-GDY, the BET (Brunauer–Emmett–Teller) surface area and pore size were determined to be 592 $m^2\ g^{-1}$ and 2.4 nm, respectively (Fig. S2a and c, ESI†), indicating the large surface area in 3D sponge-like porous Pyr-GDY. In addition, CO_2 adsorption experiment at 300 K revealed a CO_2 uptake capacity of 9.6 $cm^3\ g^{-1}$ for Cu/Pyr-GDY (Fig. S2a and b, ESI†), indicating the strong CO_2 gas affinity of 3D sponge-like porous Pyr-GDY.

The reaction of Cu/Pyr-GDY with an aqueous solution of $AgNO_3$ to get Ag/Pyr-GDY, in which the following metal displacement reaction may occur:

$$\text{Cu/Pyr-GDY} + Ag^+ \rightarrow \text{Ag/Pyr-GDY} + Cu^{2+}$$

The concentrations of $AgNO_3$ solution were varied so as to obtain Ag/Pyr-GDY composites with different amounts of Ag loading (Table S1, ESI†). Notably, for different samples obtained, the Ag content increased with the decreasing Cu content, suggesting a metal displacement process for Ag deposition (Fig. 1b). The resulting composites are denoted as Ag/Pyr-GDY-*x*, where *x* represents the mass loading of Ag (in percentage, see Table S1, ESI†). We selected Ag/Pyr-GDY-5.3 as a representative catalyst for structural characterization studies. Similar to that of Cu/Pyr-GDY, the SEM image of Ag/Pyr-GDY-5.3 also shows a 3D sponge-like morphology composed of cross-connected nanowires (Fig. 2b). The HRTEM images of Ag/Pyr-GDY-5.3 clearly display the Ag NPs on the surface of Pyr-GDY (Fig. 2c, d and Fig. S3a, ESI†). The average size of Ag NPs in Ag/Pyr-GDY-5.3 is 1.6 nm, which is larger than those of Cu NPs in Cu/Pyr-GDY (less than 1.0 nm), indicating that the Ag NPs grow larger during the metal displacement reaction. A shown in Fig. 2d, a clear lattice fringe of 0.236 nm corresponding to the (111) crystalline planes of Ag was observed in the HRTEM image of Ag/Pyr-GDY-5.3. In addition, the HAADF-STEM elemental mapping images revealed that C, Ag and Cu coexist in Ag/Pyr-GDY-5.3 (Fig. 2e–h). The results of ICP-MS measurements also demonstrate that Cu coexists with Ag NPs in Ag/Pyr-GDY-5.3 and the other Ag/Pyr-GDY-*x* samples (see Table S1, ESI†), and 0.8% Cu still coexists with Ag NPs in Ag/Pyr-GDY-24.6 even 24.6% Ag being loaded, and no obvious Cu NPs can be observed in Ag/Pyr-GDY-*x* (Fig. 2 and Fig. S3, ESI†), indicating that the metal displacement reaction mainly occured with Cu NPs in Cu/Pyr-GDY, and the Cu single atoms in Cu/Pyr-GDY is difficult to replace by Ag. Moreover, the sizes of Ag NPs become larger (3–4 nm) along with increasing amounts of Ag loading (Fig. S3, ESI†). To deeply understand the metal displacement process, Cu was completed removed by the reaction of Cu/Pyr-GDY with $FeCl_3$ soultion to get Cu-free Pyr-GDY. Though the reaction of Pyr-GDY with $AgNO_3$ can also generate Ag/Pyr-GDY-*x*, the amount of Ag loading is much smaller than the those of the reaction of Cu/Pyr-GDY under the same concentration of $AgNO_3$ (see Table S1, ESI†), indicating that the presence of Cu NPs in Cu/Pyr-GDY is benefits the Ag loading throughout the metal displacement reaction.

The XRD pattern of Ag/Pyr-GDY-5.3 (Fig. S4a, ESI†) shows an intense diffraction peak at 38.17°, corresponding to the (111) reflection of the Ag crystal surface, and the other three smaller peaks at 44.36°, 64.46° and 77.46° correspond to (200), (220), and (311) reflections of Ag crystal surfaces, respectively. The Raman spectrum of Ag/Pyr-GDY-5.3 shows five peaks at 1249, 1367, 1497, 1610 and 2189 cm^{-1}, respectively (Fig. S4b, ESI†), in which the peak at 2189 cm^{-1} represents the conjugated diacetylene links. Compared with that of Cu/Pyr-GDY (at 2178 cm^{-1}), the peak of Ag/Pyr-GDY-5.3 shifts to a higher wavenumber by $\sim$10 cm^{-1}, which might be due to the stronger interactions between Ag NPs and Pyr-GDY. The C 1s XPS spectrum of Ag/Pyr-GDY-5.3 (Fig. S4c, ESI†) is similar to that of Cu/Pyr-GDY (Fig. S1k, ESI†), indicating the anchored sites of Ag NPs in Ag/Pyr-GDY-5.3 are the same as those of Cu NPs in Cu/Pyr-GDY. The XPS spectrum of Ag 3d in Ag/Pyr-GDY-5.3 (Fig. S4d, ESI†) shows two peaks at 368.7 and 374.7 eV, respectively, corresponding to $3d_{5/2}$ and $3d_{3/2}$ electronic states of Ag(I).[70] The N_2 adsorption experiment was also carried out at 77 K for Ag/Pyr-GDY-5.3, and the BET surface area of Ag/Pyr-GDY-5.3 was determined to be only 134.2 $m^2\ g^{-1}$, much smaller than that of Cu/Pyr-GDY (592 $m^2\ g^{-1}$). In addition, the pore size in Ag/Pyr-GDY-5.3 (2.0 nm, Fig. S2f, ESI†) is also smaller than that of Cu/Pyr-GDY (2.4 nm), indicating that the framework of 3D Pyr-GDY shrinks after the formation of Ag/Pyr-GDY-5.3 to generate a smaller pores, probably due to the strong crosslinking between Ag NPs and 1D nanowires in 3D Ag/Pyr-GDY-5.3. The CO_2 adsorption experiment at 300 K revealed a CO_2 uptake capacity of 6.1 $cm^3\ g^{-1}$ for Ag/Pyr-GDY (Fig. S2e, ESI†), indicating the 3D sponge-like porous Pyr-GDY shows strong affinity towards CO_2 gas.

The catalytic performance

After understanding the structures of Ag/Pyr-GDY-*x*, we assessed their catalytic performances for the cycloaddition reactions of benzylprop-2-ynylamine (**1a**) with CO_2. First, we investigated the reaction of **1a** (0.2 mmol) with CO_2 in the presence of Ag/Pyr-GDY-24.6 (0.017 mol% based on Ag) and DBU (10 mol%, as additive) in THF (0.5 mL) for 6 h at room temperature. The product 5-methylene-3-(phenylmethyl)-2-oxazolidinone (**2a**) was successfully obtained with 100% conversion, as determined by ^{1}H NMR spectroscopy (Table 1, entry 1). The other Ag/Pyr-GDY-*x* catalysts with different Ag loadings were also assessed under the same conditions. We found that when $x \geq 5.3$, the conversion approached 100% (Table 1, entries 2–4). When $x \leq 4.4$, the conversion dropped to below 70% (Table 1, entries 5–7). When dichloromethane (DCM), acetonitrile (MeCN) and toluene were used as the solvents, the yields were lowered to 34%, 52% and 76%, respectively (Table 1, entries 8–10). It is noteworthy that **1a** could be completely converted into **2a** within 2 h even without any solvents (Table 1, entry 11). When additives other than DBU were used, no product was detected (Table 1, entries 12–14), indicating the essential role of DBU. When the amount of DBU was lowered from 10 mol% to 5 mol%, the yield of **2a** decreased to 69% (Table 1, entry 15). For comparison, the as-prepared

Table 1 Conditions screening for the reactions of **1a** with CO_2[a]

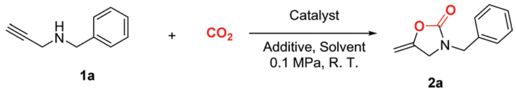

Entry	Catalyst [mol%]	Additive [mol%]	Solvent [mL]	Time [h]	Yield[b] [%]
1	Ag/Pyr-GDY-24.6[c]	DBU (10 mol%)	THF (0.5)	6	100
2	Ag/Pyr-GDY-19.5[d]	DBU (10 mol%)	THF (0.5)	6	100
3	Ag/Pyr-GDY-12.0[e]	DBU (10 mol%)	THF (0.5)	6	100
4	Ag/Pyr-GDY-5.3	DBU (10 mol%)	THF (0.5)	6	99
5	Ag/Pyr-GDY-4.4[f]	DBU (10 mol%)	THF (0.5)	6	70
6	Ag/Pyr-GDY-3.1[g]	DBU (10 mol%)	THF (0.5)	6	57
7	Ag/Pyr-GDY-2.8[h]	DBU (10 mol%)	THF (0.5)	6	49
8	Ag/Pyr-GDY-5.3	DBU (10 mol%)	DCM (0.5)	6	34
9	Ag/Pyr-GDY-5.3	DBU (10 mol%)	MeCN (0.5)	6	52
10	Ag/Pyr-GDY-5.3	DBU (10 mol%)	Toluene (0.5)	6	76
11	Ag/Pyr-GDY-5.3	DBU (10 mol%)	Solvent-free	2	100
12	Ag/Pyr-GDY-5.3	$KHCO_3$ (10 mol%)	Solvent-free	2	0
13	Ag/Pyr-GDY-5.3	Na_2SO_4 (10 mol%)	Solvent-free	2	0
14	Ag/Pyr-GDY-5.3	TEA (10 mol%)	Solvent-free	2	0
15	Ag/Pyr-GDY-5.3	DBU (5 mol%)	Solvent-free	2	69
16	Cu/Pyr-GDY[i]	DBU (10 mol%)	Solvent-free	2	0
17	Ag/Pyr-GDY-6.0 (Cu-free)[j]	DBU (10 mol%)	Solvent-free	2	97
18	AgNO[k]	DBU (10 mol%)	Solvent-free	2	23
19	$AgBF_4$[k]	DBU (10 mol%)	Solvent-free	2	25
20	AgOTf[k]	DBU (10 mol%)	Solvent-free	2	13

[a] Reaction conditions: **1a** (0.2 mmol), 0.1 MPa CO_2, catalyst (1.5 mg, 0.0036 mol% based on Ag for Ag/Pyr-GDY-5.3), additive (10 mol%, 0.02 mmol), solvent, room temperature. [b] Yields were determined by ^{1}H NMR using 1,3,5-trimethoxybenzene as the internal standard. [c] Catalyst (1.5 mg, 0.0171 mol% based on Ag). [d] Catalyst (1.5 mg, 0.0135 mol% based on Ag). [e] Catalyst (1.5 mg, 0.0084 mol% based on Ag). [f] Catalyst (1.5 mg, 0.0030 mol% based on Ag). [g] Catalyst (1.5 mg, 0.0021 mol% based on Ag). [h] Catalyst (1.5 mg, 0.0020 mol% based on Ag). [i] Catalyst (1.5 mg, 0.0160 mol% based on Cu). [j] Catalyst (1.5 mg, 0.0042 mol% based on Ag). [k] Catalyst (0.0036 mol% based on Ag).

Cu/Pyr-GDY (without Ag) and the aforementioned Ag/Pyr-GDY-6.0 (Cu-free) were also examined. Cu/Pyr-GDY gave no products (Table 1, entry 16), whereas Ag/Pyr-GDY-6.0 (Cu-free) gave a conversion of 97% (Table 1, entry 17). These results indicate that Ag might be the solely catalytic active sites. In addition, $AgNO_3$, $AgBF_4$, AgOTf were found to give rather low yields of **2a** (Table 1, entries 18–20). The above results reveal that the optimum conditions for this reaction were **1a** with 10 mol% DBU in the presence of Ag/Pyr-GDY-5.3 in a solvent-free system for 2 h under ambient temperature and pressure.

When Ag/Pyr-GDY-5.3 catalyst was filtered out after 1 h reaction, we found that the conversion showed no further increase thereafter (Fig. S5, ESI†), indicating that the reaction was catalyzed in a heterogeneous way over the Ag NPs, and no Ag leached into the solution. The recyclability of Ag/Pyr-GDY-5.3 was studied by running the reactions for five cycles, and the yields were in the range of 93–100% (Fig. S6, ESI†). The recycled Ag/Pyr-GDY-5.3 catalyst was examined by HRTEM, XPS and XRD, and no significant change was found (Fig. S7, ESI†), indicating the robustness of Ag/Pyr-GDY composite catalysts. Notably, the model reaction (catalyzed by Ag/Pyr-GDY-5.3) was scaled up, and the record TONs of 10 971 (100% conversion, entry 5, Table S2, ESI†) and 20 488 (83% conversion, entry 11, Table S2, ESI†) were obtained, which are over one order of magnitude higher than those of the reported state-of-the-art catalysts (Fig. 3 and Table S3, ESI†), indicating the outstanding catalytic activity of Ag/Pyr-GDY-5.3. Such a high catalytic activity can be attributed to following aspects: (1) the porous sponge-like 3D Pyr-GDY component can anchor and stabilize the capping agent free ultrafine Ag NPs through the strong interactions between alkynyl groups and Ag, and the capping agent free ultrafine Ag NPs can efficiently bind and activate the acetylene bond of propargylamines, which greatly promote the CO_2 cycloaddition reactions. (2) The nature of porous sponge-like 3D Pyr-GDY benefits the mass transfer and

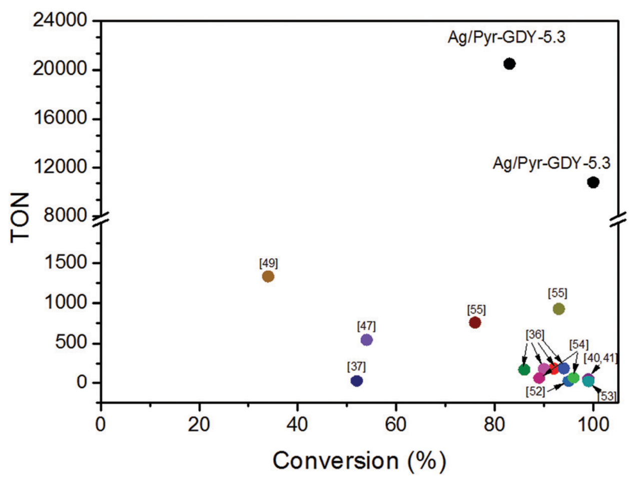

Fig. 3 A comparison of TONs and conversions for Ag–Pyr-GDY-5.3 with those of the Ag-based state-of-the-art catalysts.

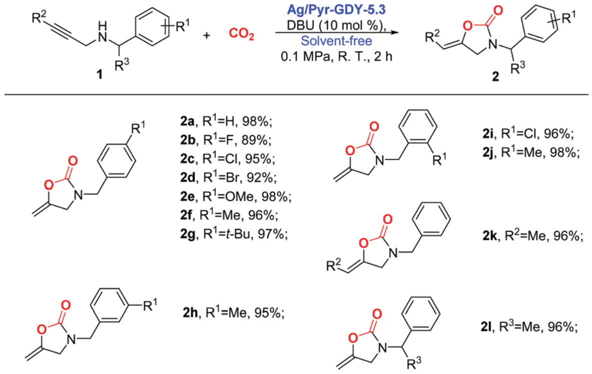

Scheme 1 Investigations on the scope of **1**.[a,b] (Reaction conditions: **1** (0.2 mmol), 0.1 MPa CO_2, catalyst (1.5 mg, 0.0036 mol% based on Ag), DBU (10 mol%, 0.02 mmol, room temperature, 2 h; the yields listed in this scheme are isolated yields.)

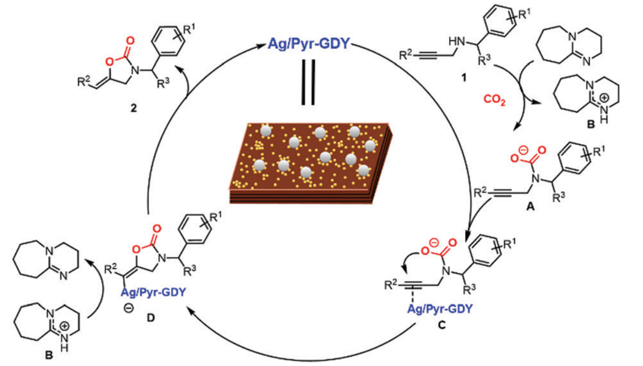

Fig. 5 The proposed reaction mechanism.

enriches both CO_2 and propargylamines within the pores of Ag/Pyr-GDY-5.3, which can also promote its catalytic efficiency. Our results demonstrate that porous sponge-like 3D Pyr-GDY is an ideal support for anchoring and stabilizing the capping agent free ultrafine metal NPs for the construction of high performance heterogeneous catalysts.

After optimizing the reaction conditions, we explored the scope of the reactions by using a series of substituted **1** (Scheme 1). When electron-withdrawing groups such as F, Cl, and Br were introduced as R^1 at the *para*-position, the corresponding products **2b**–**2d** were isolated in 89–95% yields. Therefore, halide substituents proved compatible with the reaction, which offers opportunities for further functionalization. When electron-donating groups were introduced instead, the products **2e**–**2g** were obtained in 96%–98% yields. When R^1 = Me at the *meta*-position, the corresponding product **2h** was isolated in 95% yield. When R^1 = Cl or Me at the *ortho*-position, the products **2i** and **2j** were obtained in 96% and 98% yields, respectively. The above results indicate that substrates with electron-donating R^1 groups would give relatively high yields compared to those with electron-withdrawing groups. We also used a substrate with R^2 = Me, and this internal alkyne could be converted into the corresponding product **2k** with an isolated yield of 96%. When R^3 = Me, the yield for **2l** was found to be 96% as well. The above results demonstrate that our catalyst of Ag/Pyr-GDY-5.3 has an excellent substrate-compatibility.

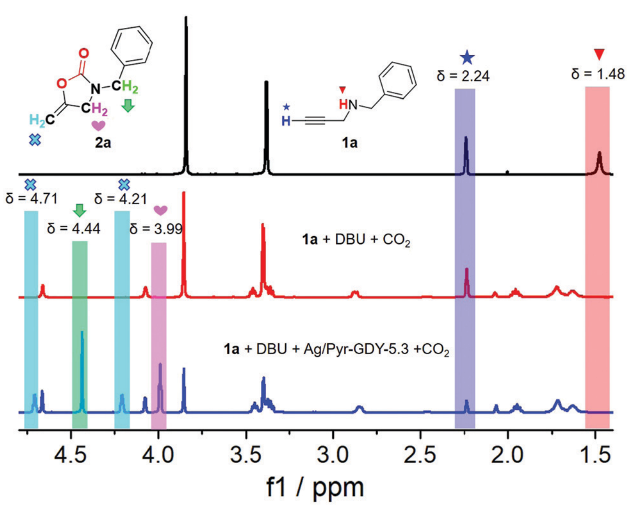

Fig. 4 ^1H NMR spectra of **1a**, **1a** + DBU + CO_2, and **1a** + DBU + CO_2 + Ag/Pyr-GDY-5.3 in $CDCl_3$.

The catalytic mechanism

To monitor the reaction process, the ^1H NMR spectra of **1a** with various reactants were obtained (Fig. 4 and Fig. S8, ESI†). As shown in Fig. S8a (ESI†), the proton signal of the amino group in **1a** displays a sharp peak at δ = 1.48 ppm, which is almost unchanged after bubbling with CO_2 (Fig. S8b, ESI†), indicating that **1a** cannot react with CO_2 in the absence of DBU and the catalyst. However, this peak completely disappeared after the addition of DBU + CO_2 (Fig. S8f, ESI†), and two new peaks at δ = 4.66 and 4.08 ppm were observed (Fig. 4). However, the proton signal of terminal alkyne in **1a**, with a sharp peak at δ = 2.24 ppm, was almost unchanged after the addition of DBU + CO_2 (Fig. 4 and Fig. S8f, ESI†), indicating that a new species of intermediate **A** (see Fig. 5) was formed. When Ag/Pyr-GDY-5.3 was added to the reaction system of **1a** + DBU + CO_2, the intensity of the peak belonging to the proton of terminal alkyne dramatically decreased (Fig. 4 and Fig. S8g, ESI†), and four additional new peaks at δ = 4.71, 4.44, 4.21, and 3.99 ppm belonging to the product **2a** appeared (Fig. 4), demonstrating **2a** can only be formed in the presence of the Ag/Pyr-GDY-5.3 catalyst. Based on the above results, a proposed catalytic mechanism is given in Fig. 5, in which the amino group in **1a** is firstly activated with the assistance of DBU, and an intermediate **A** is generated from the reaction of **1a** with CO_2. Subsequently, the alkynyl group in **A** is activated by the coordination interaction between the alkynyl group and Ag NPs in Ag/Pyr-GDY-5.3 to generate the intermediate **C**, and then **C** undergoes an intramolecular nucleophilic attack of CO_2^- group to the activated carbon of alkynyl group to generate **D**, and **D** obtains a proton from the protonated DBU to generate the product of **2a**.

3. Conclusions

In summary, we have synthesized a series of Ag/Pyr-GDY composite catalysts by a simple metal displacement reaction, in which the surface capping agent free ultrafine Ag NPs can be anchored and stabilized by a unique 3D sponge-like porous Pyr-GDY carbon support, through the strong affinity of Ag NPs towards the alkynyl groups in Pyr-GDY. With an optimized Ag loading, the composite catalyst displays a record-high catalytic performance for the cycloaddition reaction of alkynyl amines with CO_2 even without any solvents. The TONs reach as high as 10 971 (TOF = 183 h^{-1}, yield = 100%) and 20 488 (TOF = 93 h^{-1}, yield = 83%), both significantly higher than that for Ag27-MOF, the most efficient heterogeneous catalyst reported thus far. The outstanding catalytic performance of Ag/Pyr-GDY can be attributed to the unique structure of 3D sponge-like porous Pyr-GDY containing plenty of alkynyl groups, which provides an ideal anchored site for the dispersion and stabilization of capping agents free ultrafine Ag NPs, and offers highly efficient catalytic sites for the activation of the alkynyl group in propargylamines. In addition, the porous sponge-like 3D Pyr-GDY also benefits mass transfer and enriches the reactants within the pores of Ag/Pyr-GDY, which further enhances its catalytic activity. Our work is a big step forward in the practical application of CCUS through an economic and green pathway. Further investigations on the catalytic performances of Pyr-GDY-based catalysts for ambient chemical fixation of CO_2 are currently underway in our laboratory.

4. Experimental section

Materials

All solvents were obtained from commercial sources and were purified according to standard procedures. Propargylic amines **1a**, **1c**, **1d**, **1e**, **1f**, **1g**, **1h**, **1j**, **1k**[40] and **1b**, **1i**, **1l**, **1m**[49] were synthesized according to the literature procedures. **SI-1** and **SI-2** were commercially available.

Instrumentation

The high-resolution transmission electron microscopy (HRTEM) images and the corresponding energy-dispersive X-ray spectroscopy (EDS) elemental mapping results were obtained on a high-resolution transmission electron microscope (Talos F200X, FEI, USA), and Mo grid rather than Cu grid was used to avoid the interference of Cu holder. The HAADF-STEM images were obtained on a transmission electron microscope with a probe corrector (Titan Themis Cubed G2 60-300, FEI). The powder X-ray diffraction (XRD) of all powders were obtained by using a Smart X-ray diffractometer (Smart Lab 9 kW, Rigaku, Japan) with Cu Kα radiation (λ = 1.54178 Å). The CO_2 sorption isotherm test was conducted on a multi-station specific surface micropore and vapor adsorption analyzer (BELSORP-Mas, Microtrac BEL, Japan). X-Ray photoelectron spectroscopy (XPS) was used to obtain spectra on a photoelectron spectrometer (ESCALAB250Xi, THERMO SCIENTIFIC, United Kingdom), and the XPS spectra were calibrated *versus* C 1s (284.8 eV) binding energy. The amounts of Ag and Cu on catalysts were determined *via* inductively coupled plasma-atomic emission spectroscopy (ICP-MS, SPECTRO-BLUE). Raman spectra were recorded on a high-resolution laser confocal fiber Raman spectrometer (HORIBA EVOLVTION, HORIBA Jobinyvon, France). The ^{1}H NMR, ^{13}C NMR and ^{19}F NMR spectra were recorded on Bruker 400 MHz spectrometer instruments in $CDCl_3$. The chemical shifts (δ) of ^{1}H NMR, ^{13}C NMR and ^{19}F NMR were measured in ppm, referenced to residual ^{1}H and ^{13}C signals of non-deuterated $CDCl_3$ (δ = 7.26 and 77.00), as internal standards. The products of catalytic reactions were purified *via* column chromatography using silica gel (200–300 mesh). Thin layer chromatography (TLC) was performed on Merck silica gel GF254 plates and visualized using UV light (254 nm).

Preparation of Cu/Pyr-GDY

Cu/Pyr-GDY was synthesized from 1,3,6,8-tetra[(trimethylsilyl) ethynyl]phrene (TEP-TMS). First, TEP-TMS (100 mg) in tetrahydrofuran (THF, 20 mL) was desilicated by tetrabutyl ammonium fluoride (TBAF, 1 M in THF, 1 mL) under a N_2 atmosphere for 15 min. The resulting mixture was washed 3 times with saturated sodium chloride solution (20 mL) and then extracted with ethyl acetate (10 mL × 3). The organic phase was dried with anhydrous Na_2SO_4, then filtered, and the solvent was removed under reduced pressure. The obtained TEP monomer was dissolved in 25 mL pyridine. Copper(II) acetate (30 mg) was dissolved in pyridine (5–10 mL) in a three-necked flask. The TEP solution was added dropwise into the flask at 110 °C, and the mixture was kept at 110 °C for 3 days. Pyridine was removed under reduced pressure. The obtained Cu/Pyr-GDY powder was washed sequentially with *N*,*N*-dimethyl formamide (DMF) and acetone to remove unreacted TEP monomers and oligomers, and then the dark brown powder was dried at 50 °C under a vacuum overnight.

Preparation of Ag/Pyr-GDY

Cu/Pyr-GDY powder (5 mg) was dispersed in $AgNO_3$ aqueous solution (1 mL) with various concentrations (see Table S1, ESI†), and sonicated for 15 s. Then the mixture was washed three times with acetone (10 mL), the powder was separated by centrifugation, and then dried at 50 °C under a vacuum overnight.

Preparation of Pyr-GDY

Cu/Pyr-GDY powder (5 mg), $FeCl_3$ solution (1 M, 10 mL), and HCl solution (0.001 M, 30 mL) were mixed in a centrifuge tube, and the mixture was stirred at room temperature for 12 h. The powder was separated *via* centrifugation, washed three times alternately by HCl (1 M, 10 mL) and acetone (10 mL), and then dried at 50 °C under a vacuum overnight. The results of ICP-MS measurements confirmed that there is no detectable copper in the as-prepared Pyr-GDY.

Preparation of Ag/Pyr-GDY (Cu-free)

Pyr-GDY powder (5 mg) was dispersed in $AgNO_3$ aqueous solution (1 mL) with various concentrations (see Table S1, ESI†), and sonicated for 15 s. The mixture was washed three times by acetone (10 mL), and the powder was separated by centrifugation, and then dried at 50 °C under a vacuum overnight.

The catalytic reactions

In a sealed reaction tube containing Ag/Pyr-GDY-*x*, 1,8-diazabicyclo[5.4.0]undec-7-ene (DBU, 0.1 equiv.) and **1a** (1.0 equiv.) was evacuated and purged with CO_2 gas three times. The tube was then connected to a balloon filled with CO_2, and the mixture therein was stirred at room temperature for a given time (see Table 1).

Author contributions

Chang Liu: experiments, data analysis. Chao Zhang: writing – review & editing. Tong-Bu Lu: supervision.

Conflicts of interest

There are no conflicts to declare.

Acknowledgements

The authors gratefully acknowledge financial support from the National Natural Science Foundation of China (21790052 and 21931007), the National Key R&D Program of China (2017YFA 0700104), and the 111 Project of China (D17003).

Notes and references

1 M. R. Allen, D. J. Frame, C. Huntingford, C. D. Jones, J. A. Lowe, M. Meinshausen and N. Meinshausen, Warming caused by cumulative carbon emissions towards the trillionth tonne, *Nature*, 2009, **458**, 1163–1166.
2 G. A. Florides and P. Christodoulides, Global warming and carbon dioxide through sciences, *Environ. Int.*, 2009, **35**, 390–401.
3 Y. Y. Birdja, E. Pérez-Gallent, M. C. Figueiredo, A. J. Göttle, F. Calle-Vallejo and M. T. M. Koper, Advances and challenges in understanding the electrocatalytic conversion of carbon dioxide to fuels, *Nat. Energy*, 2019, **4**, 732–745.
4 A. D. Handoko, F. Wei, Jenndy, B. S. Yeo and Z. W. She, Understanding heterogeneous electrocatalytic carbon dioxide reduction through operando techniques, *Nat. Catal.*, 2018, **1**, 922–934.
5 M. B. Ross, P. D. Luna, Y. Li, C.-T. Dinh, D. Kim, P. Yang and E. H. Sargent, Designing materials for electrochemical carbon dioxide recycling, *Nat. Catal.*, 2019, **2**, 648–658.
6 S. Nitopi, E. Bertheussen, S. B. Scott, X. Liu, A. K. Engstfeld, S. Horch, B. Seger, I. E. L. Stephens, K. Chan, C. Hahn, J. K. Nørskov, T. F. Jaramillo and I. Chorkendorff, Progress and Perspectives of Electrochemical CO_2 Reduction on Copper in Aqueous Electrolyte, *Chem. Rev.*, 2019, **119**, 7610–7672.
7 D. Gao, R. M. Arán-Ais, H. S. Jeon and B. R. Cuenya, Rational catalyst and electrolyte design for CO_2 electroreduction towards multicarbon products, *Nat. Catal.*, 2012, **2**, 198–210.
8 Y. Liu, D. Tian, A. N. Biswas, Z. Xie, S. Hwang, J. H. Lee, H. Meng and J. G. Chen, Transition Metal Nitrides as Promising Catalyst Supports for Tuning CO/H_2 Syngas Production from Electrochemical CO_2 Reduction, *Angew. Chem., Int. Ed.*, 2020, **132**, 11441–11444.
9 S. Garg, M. Li, A. Z. Weber, L. Ge, L. Li, V. Rudolph, G. Wang and T. E. Rufford, Advances and challenges in electrochemical CO_2 reduction processes: an engineering and design perspective looking beyond new catalyst materials, *J. Mater. Chem. A*, 2020, **8**, 1511–1544.
10 W. Choi, D. H. Won and Y. J. Hwang, Catalyst design strategies for stable electrochemical CO_2 reduction reaction, *J. Mater. Chem. A*, 2020, **8**, 15341–15357.
11 R. Xia, S. Zhang, X. Ma and F. Jiao, Surface-functionalized palladium catalysts for electrochemical CO_2 reduction, *J. Mater. Chem. A*, 2020, **8**, 15884–15890.
12 M. G. Kibria, J. P. Edwards, C. M. Gabardo, C.-T. Dinh, A. Seifitokaldani, D. Sinton and E. H. Sargent, Electrochemical CO_2 Reduction into Chemical Feedstocks: From Mechanistic Electrocatalysis Models to System Design, *Adv. Mater.*, 2019, **31**, 1807166.
13 S. Xu and E. A. Carter, Theoretical Insights into Heterogeneous (Photo)electrochemical CO_2 Reduction, *Chem. Rev.*, 2019, **119**, 6631–6669.
14 K. Maeda, Metal-Complex/Semiconductor Hybrid Photocatalysts and Photoelectrodes for CO_2 Reduction Driven by Visible Light, *Adv. Mater.*, 2019, **31**, 1808205.
15 Y. Jiang, J.-F. Liao, H.-Y. Chen, H.-H. Zhang, J.-Y. Li, X.-D. Wang and D.-B. Kuang, All-Solid-State Z-Scheme α-Fe_2O_3/Amine-RGO/$CsPbBr_3$ Hybrids for Visible-Light-Driven Photocatalytic CO_2 Reduction, *Chem*, 2020, **6**, 766–780.
16 H. S. Lee, S. Jee, R. Kim, H.-T. Bui, B. Kim, J.-K. Kim, K. S. Park, W. Choi, W. Kim and K. M. Choi, A highly active, robust photocatalyst heterogenized in discrete cages of metal–organic polyhedra for CO_2 reduction, *Energy Environ. Sci.*, 2020, **13**, 519–526.
17 J. Li, F. Wei, C. Dong, W. Mu and X. Han, A Z-scheme $ZnFe_2O_4$/RGO/In_2O_3 hierarchical photocatalyst for efficient CO_2 reduction enhancement, *J. Mater. Chem. A*, 2020, **8**, 6524–6531.
18 X. Xiong, Y. Zhao, R. Shi, W. Yin, Y. Zhao, G. I. N. Waterhouse and T. Zhang, Selective photocatalytic CO_2 reduction over Zn-based layered double hydroxides containing tri or tetravalent metals, *Sci. Bull.*, 2020, **65**, 987–994.
19 Y. Zhang, B. Xia, J. Ran, K. Davey and S. Z. Qiao, Atomic-Level Reactive Sites for Semiconductor-Based Photocatalytic CO_2 Reduction, *Adv. Energy Mater.*, 2020, **10**, 1903879.
20 S. Hu, L. Ma, F. Li, Z. Fan, Q. Wang, J. Bai, X. Kang and G. Wu, Construction of g-C_3N_4/S-g-C_3N_4 metal-free isotype heterojunctions with an enhanced charge driving force and

their photocatalytic performance under anoxic conditions, *RSC Adv.*, 2015, **5**, 90750–90756.

21 L. Wang, W. Chen, D. Zhang, Y. Du, R. Amal, S. Qiao, J. Wu and Z. Yin, Surface strategies for catalytic CO_2 reduction: from two-dimensional materials to nanoclusters to single atoms, *Chem. Soc. Rev.*, 2019, **48**, 5310–5349.

22 M. R. Ding, W. Flaig, H.-L. Jiang and O. M. Yaghi, Carbon capture and conversion using metal–organic frameworks and MOF-based materials, *Chem. Soc. Rev.*, 2019, **48**, 2783–2828.

23 F. L. Sousa, M. Preiner and W. F. Martin, Native metals, electron bifurcation, and CO_2 reduction in early biochemical evolution, *Curr. Opin. Microbiol.*, 2018, **43**, 77–83.

24 Y.-X. Huang and Z. Hu, An integrated electrochemical and biochemical system for sequential reduction of CO_2 to methane, *Fuel*, 2018, **220**, 8–13.

25 P. R. Yaashikaa, P. S. Kumar, S. J. Varjani and A. Saravanan, A review on photochemical, biochemical and electrochemical transformation of CO_2 into value-added products, *J. CO2 Util.*, 2019, **33**, 131–147.

26 L. Ma, L. Zhou, S. M. Mbadinga, J.-D. Gu and B.-Z. Mu, Accelerated CO_2 reduction to methane for energy by zero valent iron in oil reservoir production waters, *Energy*, 2018, **147**, 663–671.

27 L.-Y. Wu, Y.-F. Mu, X.-X. Guo, W. Zhang, Z.-M. Zhang, M. Zhang and T.-B. Lu, Encapsulating Perovskite Quantum Dots in Iron-Based Metal–Organic Frameworks (MOFs) for Efficient Photocatalytic CO_2 Reduction, *Angew. Chem., Int. Ed.*, 2019, **58**, 9491–9495.

28 T. Ouyang, H.-H. Huang, J.-W. Wang, D.-C. Zhong and T.-B. Lu, A Dinuclear Cobalt Cryptate as a Homogeneous Photocatalyst for Highly Selective and Efficient Visible-Light Driven CO_2 Reduction to CO in CH_3CN/H_2O Solution, *Angew. Chem., Int. Ed.*, 2017, **56**, 738–743.

29 T. Ouyang, H.-J. Wang, H.-H. Huang, J.-W. Wang, S. Guo, W.-J. Liu, D.-C. Zhong and T.-B. Lu, Dinuclear Metal Synergistic Catalysis Boosts Photochemical CO_2-to-CO Conversion, *Angew. Chem., Int. Ed.*, 2018, **57**, 16480–16485.

30 X. Rong, H.-J. Wang, X.-L. Lu, R. Si and T.-B. Lu, Control Synthesis of Vacancy-Defect Single-Atom Catalyst for Boosting CO_2 Electroreduction, *Angew. Chem., Int. Ed.*, 2020, **132**, 1977–1981.

31 D. J. Darensbourg, Making Plastics from Carbon Dioxide: Salen Metal Complexes as Catalysts for the Production of Polycarbonates from Epoxides and CO_2, *Chem. Rev.*, 2007, **107**, 2388–2410.

32 X. B. Lu, W. M. Ren and G. P. Wu, CO_2 Copolymers from Epoxides: Catalyst Activity, Product Selectivity, and Stereochemistry Control, *Acc. Chem. Res.*, 2012, **45**, 1721–1735.

33 S. Pulla, C. M. Felton, P. Ramidi, Y. Gartia, N. Ali, U. B. Nasini and A. Ghosh, Advancements in oxazolidinone synthesis utilizing carbon dioxide as a C1 source, *J. CO2 Util.*, 2013, **2**, 49–57.

34 T. Niemi, J. E. Perea-Buceta, I. Fernandez, S. Alakurtti, E. Rantala and T. Repo, Direct Assembly of 2-Oxazolidinones by Chemical Fixation of Carbon Dioxide, *Chem. – Eur. J.*, 2014, **20**, 8867–8871.

35 M. Y. Wang, Q. W. Song, R. Ma, J. N. Xie and L. N. He, Efficient conversion of carbon dioxide at atmospheric pressure to 2-oxazolidinones promoted by bifunctional Cu(II)-substituted polyoxometalate-based ionic liquids, *Green Chem.*, 2016, **18**, 282–287.

36 M. Yoshida, T. Mizuguchi and K. Shishido, Synthesis of Oxazolidinones by Efficient Fixation of Atmospheric CO_2 with Propargylic Amines by using a Silver/1,8-Diazabicyclo [5.4.0]undec-7-ene (DBU) Dual-Catalyst System, *Chemistry*, 2012, **18**, 15578–15581.

37 S. Hase, Y. Kayaki and T. Ikariya, NHC–Gold(I) Complexes as Effective Catalysts for the Carboxylative Cyclization of Propargylamines with Carbon Dioxide, *Organometallics*, 2013, **32**, 5285–5288.

38 Y. Zhao, J. Qiu, L. Tian, Z. Li, M. Fan and J. Wang, New Copper(I)/DBU Catalyst System for the Carboxylative Cyclization of Propargylic Amines with Atmospheric CO_2: An Experimental and Theoretical Study, *ACS Sustainable Chem. Eng.*, 2016, **4**, 5553–5560.

39 G. Zhang, H. Yang and H. Fei, Unusual Missing Linkers in an Organosulfonate-Based Primitive–Cubic (pcu)-Type Metal–Organic Framework for CO_2 Capture and Conversion under Ambient Conditions, *ACS Catal.*, 2018, **8**, 2519–2525.

40 Z.-H. Zhou, K.-H. Chen and L.-N. He, Efficient and Recyclable Cobalt(II)/Ionic Liquid Catalytic System for CO_2 Conversion to Prepare 2-Oxazolinones at Atmospheric Pressure, *Chin. J. Chem.*, 2019, **37**, 1223–1228.

41 C.-S. Cao, S.-M. Xia, Z.-J. Song, H. Xu, Y. Shi, L.-N. He, P. Cheng and B. Zhao, Highly Efficient Conversion of Propargylic Amines and CO_2 Catalyzed by Noble-Metal-Free [Zn_{116}] Nanocages, *Angew. Chem., Int. Ed.*, 2020, **59**, 8586–8593.

42 M. Shi and Y. M. Shen, Transition-Metal-Catalyzed Reactions of Propargylamine with Carbon Dioxide and Carbon Disulfide, *J. Org. Chem.*, 2002, **67**, 16–21.

43 P. García-Domínguez, L. Fehr, G. Rusconi and C. Nevado, Palladium-catalyzed incorporation of atmospheric CO_2: efficient synthesis of functionalized oxazolidinones, *Chem. Sci.*, 2016, **7**, 3914–3918.

44 A. Bacchi, G. P. Chiusoli, M. Costa, B. Gabriele, C. Righi and G. Salerno, Palladium-catalysed sequential carboxylation–alkoxycarbonylation of acetylenic amines, *Chem. Commun.*, 1997, 1209–1210.

45 S. Ghosha, S. Riyajuddinb, S. Sarkara, K. Ghoshb and S. M. Islam, Pd NPs Decorated on POPs as Recyclable Catalysts for the Synthesis of 2-Oxazolidinones from Propargylic Amines via Atmospheric Cyclizative CO_2 Incorporation, *ChemNanoMat*, 2020, **6**, 160–172.

46 S. M. Sadeghzadeh, R. Zhiani and S. Emrani, Ni@Pd nanoparticles supported on ionic liquid-functionalized KCC-1 as robust and recyclable nanocatalysts for cycloaddition of propargylic amines and CO_2, *Appl. Organomet. Chem.*, 2018, **32**, e3941.

47 Q. W. Song and L. N. He, Robust Silver(I) Catalyst for the Carboxylative Cyclization of Propargylic Alcohols with Carbon Dioxide under Ambient Conditions, *Adv. Synth. Catal.*, 2016, **358**, 1251–1258.

48 A. H. Liu, R. Ma, C. Song, Z. Z. Yang, A. Yu, Y. Cai, L. N. He, Y. N. Zhao, B. Yu and Q. W. Song, Equimolar CO_2 Capture by N-Substituted Amino Acid Salts and Subsequent Conversion, *Angew. Chem., Int. Ed.*, 2012, **51**, 11306–11310.

49 M. Zhao, S. Huang, Q. Fu, W. Li, R. Guo, Q. Yao, F. Wang, P. Cui, C.-H. Tung and D. Sun, Ambient Chemical Fixation of CO_2 Using a Robust Ag_{27} Cluster-Based Two-Dimensional Metal–Organic Framework, *Angew. Chem., Int. Ed.*, 2020, **59**, 20031–20036.

50 S. Kikuchi, S. Yoshida, Y. Sugawara, W. Yamada, H.-M. Cheng, K. Fukui, K. Sekine, I. Iwakura, T. Ikeno and T. Yamada, Silver-Catalyzed Carbon Dioxide Incorporation and Rearrangement on Propargylic Derivatives, *Bull. Chem. Soc. Jpn.*, 2011, **84**, 698–717.

51 S. Yoshida, K. Fukui, S. Kikuchi and T. Yamada, Silver-catalyzed Preparation of Oxazolidinones from Carbon Dioxide and Propargylic Amines, *Chem. Lett.*, 2009, **38**, 786–787.

52 X. Wang, Z. Chang, X. Jing, C. He and C. Duan, Double-Helical Ag–S Rod-Based Porous Coordination Polymers with Double Activation: σ-Active and π-Active Functions, *ACS Omega*, 2019, **4**, 10828–10833.

53 H. Yang, X. Zhang, G. Zhang and H. Fei, An alkaline-resistant Ag(I)-anchored pyrazolate-based metal-organic framework for chemical fixation of CO_2, *Chem. Commun.*, 2018, **54**, 4469–4472.

54 S. Ghosh, T. S. Khan, A. Ghosh, A. H. Chowdhury, M. A. Haider, A. Khan and S. M. Islam, Utility of Silver Nanoparticles Embedded Covalent Organic Frameworks as Recyclable Catalysts for the Sustainable Synthesis of Cyclic Carbamates and 2-Oxazolidinones via Atmospheric Cyclizative CO_2 Capture, *ACS Sustainable Chem. Eng.*, 2020, **8**, 5495–5513.

55 Z. Chang, X. Jing, C. He, X. Liu and C. Duan, Silver Clusters as Robust Nodes and π–Activation Sites for the Construction of Heterogeneous Catalysts for the Cycloaddition of Propargylamines, *ACS Catal.*, 2018, **8**, 1384–1391.

56 S. Ghosh, R. A. Molla, U. Kayal, A. Bhaumik and S. M. Islam, Ag NPs decorated on a COF in the presence of DBU as an efficient catalytic system for the synthesis of tetramic acids *via* CO_2 fixation into propargylic amines at atmospheric pressure, *Dalton Trans.*, 2019, **48**, 4657–4666.

57 P. Bhanja, A. Modak and A. Bhaumik, Supported Porous Nanomaterials as Efficient Heterogeneous Catalysts for CO_2 Fixation Reactions, *Chem. – Eur. J.*, 2018, **24**, 7278–7297.

58 K. Fujita, K. Inoue, J. Sato, T. Tsuchimoto and H. C. Yasuda, Carboxylative cyclization of propargylic amines with CO_2 catalyzed by dendritic N-heterocyclic carbene-gold(I) complexes, *Tetrahedron*, 2016, **72**, 1205–1212.

59 K. Yamashita, S. Hase, Y. Kayaki and T. Ikariya, Highly Selective Carboxylative Cyclization of Allenylmethylamines with Carbon Dioxide Using N-Heterocyclic Carbene-Silver(I) Catalysts, *Org. Lett.*, 2015, **17**, 2334–2337.

60 S. M. Sadeghzadeh, Gold(III) phosphorus complex immobilized on fibrous nano-silica as a catalyst for the cyclization of propargylic amines with CO_2, *J. Mol. Catal. A: Chem.*, 2016, **423**, 216–223.

61 S. M. Sadeghzadeh, A green approach for the synthesis of 2-oxazolidinones using gold(I) complex immobilized on KCC-1 as nanocatalyst at room temperature, *Appl. Organometal. Chem.*, 2016, **30**, 835–842.

62 H. Matsuo, A. Fujii, J.-C. Choi, T. Fujitani and K. Fujita, Carboxylative Cyclization of Propargylic Amines with Carbon Dioxide-Catalyzed by Poly(amidoamine)-Dendrimer-Encapsulated Gold Nanoparticles, *Synlett*, 2019, 1914–1918.

63 F. Inagaki, K. Maeda, K. Nakazawa and C. Mukai, Construction of the Oxazolidinone Framework from Propargylamine and CO_2 in Air at Ambient Temperature: Catalytic Effect of a Gold Complex Featuring an L_2/Z-Type Ligand, *Eur. J. Org. Chem.*, 2018, 2972–2976.

64 G. Li, Y. Li, H. Liu, Y. Gao, Y. Li and D. Zhu, Architecture of graphdiyne nanoscale films, *Chem. Commun.*, 2010, **46**, 3256–3258.

65 S. Zhan, Y. Zhao, N. Yang and D. Wang, Pore Structure of Graphdiyne: Design, Synthesis and Application, *Chem. J. Chin. Univ.*, 2021, **42**, 333–348.

66 J. Li, C. Wan, C. Wang, H. Zhang and X. Chen, 2D Material Chemistry: Graphdiyne-based Biochemical Sensing, *Chem. Res. Chin. Univ.*, 2020, **36**, 622–630.

67 L.-L. Yang, H.-J. Wang, J. Wang, Y. Li, W. Zhang and T.-B. Lu, A graphdiyne-based carbon material for electroless deposition and stabilization of sub-nanometric Pd catalysts with extremely high catalytic activity, *J. Mater. Chem. A*, 2019, **7**, 13142–13148.

68 M. Li, H.-J. Wang, C. Zhang, Y.-B. Chang, S.-J. Li, W. Zhang and T.-B. Lu, Enhancing the photoelectrocatalytic performance of metal-free graphdiyne-based catalyst, *Sci. China: Chem.*, 2020, **63**, 1040–1045.

69 J. Kim, W. Choi, J. W. Park, C. Kim, M. Kim and H. Song, Branched Copper Oxide Nanoparticles Induce Highly Selective Ethylene Production by Electrochemical Carbon Dioxide Reduction, *J. Am. Chem. Soc.*, 2019, **141**, 6986–6994.

70 G. Corroa, E. Vidal, S. Cebadaa, U. Pal, F. Banuelos, D. Vargas and E. Guilleminot, Electronic state of silver in Ag/SiO_2 and Ag/ZnO catalysts and its effect on diesel particulate matter oxidation: An XPS study, *Appl. Catal., B*, 2017, **216**, 1–10.

